Light-Controlled Morphologies of Self-Assembled Triarylamine–Fullerene Conjugates

Eric Busseron,[†] Juan-José Cid,[†] Adrian Wolf,[†] Guangyan Du,[†] Emilie Moulin,[†] Gad Fuks,[†] Mounir Maaloum,[†] Prasad Polavarapu,[†] Adrian Ruff,[‡] Ann-Kathrin Saur,[‡] Sabine Ludwigs,[‡] and Nicolas Giuseppone*,[†]

[†]SAMS Research Group, University of Strasbourg, Institut Charles Sadron, CNRS, 23 rue du Loess, BP 84087, Strasbourg 67034 Cedex 2, France and [‡]Institut für Polymerchemie, Universität Stuttgart, Pfaffenwaldring 55, Stuttgart 70569, Germany

ABSTRACT A family of triarylamine–fullerene conjugates has been synthesized and shown to self-assemble upon light stimulation in chlorinated solvents. This light-induced process primarily involves excitation of triarylamine derivatives, which then oxidize and stack with their neutral counterparts to form charge transfer complexes in the form of p-conducting channels, while fullerenes are consequently enforced in coaxial n-conducting columnar arrangements. These supramolecular heterojunctions can be organized over very long distances in micrometric fibers when a controlled amount of photons is provided from a white light source to initiate the process. Surprisingly, when sunlight or UV light is used instead, the nanostructuration leads to monodisperse spherical objects due to the nature of the nucleation–growth process involved in the stacks formation. This control over the supramolecular morphology of organic self-assemblies using the nature of light is of general interest for the design of functional responsive materials.

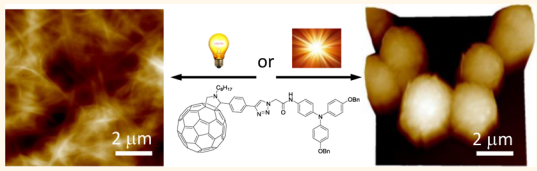

KEYWORDS: nanostructures · responsive self-assemblies · supramolecular polymers · triarylamine · fullerene

Control over nano- and microstructuration of supramolecular polymers and self-assemblies is of high importance for their implementation as functional materials.[1−4] From a fundamental point of view, self-assembly triggered and controlled by noninvasive light stimulation is of interest to understand and to make use of structure/function relationships at various length scales of organization. Aggregated systems in which structural (size, shape) and functional (conductivity, wettability, permeability) properties can be changed by light are of high potential for applications, going from optics and electronics to diagnostics and therapeutics. In particular, light-responsive materials are currently intensively studied in the fields of polymer science[5−7] and of organic supramolecular chemistry[8−11] by taking advantage of photoisomerizable units such as azobenzene. With the use of totally different mechanisms based on nucleation/growth processes, variations of light intensity or wavelength can also modulate the shape and properties of inorganic nanoparticles.[12−15] However, to the best of our knowledge, such light-controlled nucleation/growth mechanisms have not yet been described for tuning the hierarchical organization of purely organic supramolecular structures.

Here we show the possibility to produce such light-controlled self-assemblies using triarylamine–fullerene conjugates. This proof of concept using donor–acceptor molecules is of general interest because the precise ordering of photo- and electroactive molecules in devices such as organic field effect transistors (OFETs), organic light emitting diodes (OLEDs), and organic photovoltaic devices (OPVs) can significantly enhance their efficiency.[16,17] For instance, in order to improve the dissociation of excitons and to reduce the recombination of charge carriers in solar cells, one can take advantage of very specific morphologies of the active layer involving supramolecular heterojunctions. This type of architecture with long-range ordering involves the columnar arrangement of well-separated electron donor and acceptor domains in the low nm range. In this configuration with coaxial hole and electron transporting channels, charges can migrate

* Address correspondence to giuseppone@unistra.fr.

Received for review November 21, 2014 and accepted March 3, 2015.

Published online March 03, 2015
10.1021/nn506646m

to the electrodes with minimal recombination losses compared to bulk heterojunctions for instance.[18−22] Such supramolecular heterojunctions often include fullerene derivatives[23] as n-type channel for electron transport and for instance porphyrin or coronene as p-type channel for hole transport.[13,14] These latter also often serve as supramolecular structuring units by enforcing the stacking of columnar aggregates. However, and although several triarylamine−fullerene conjugates have been reported in the literature and show very promising ambipolar characteristics,[24−34] the self-assembly of these derivatives into supramolecular heterojunctions has never been achieved, probably because triarylamines themselves were not known to produce any type of supramolecular organization.[35−39] Recently we have discovered that, by introducing appropriate lateral groups in triarylamine derivatives, it becomes possible to trigger their supramolecular polymerization in columnar systems[40−43] showing outstanding hole conduction properties with optical, magnetic, and electronic behavior of metallic materials.[44,45] Light-triggered self-assembled triarylamines were subsequently used for the first time in OPVs by the group of Kumar with enhanced photovoltaic efficiency[46] and exceptional theoretical mobilities as high as 12 $cm^2\ V^{-1}\ s^{-1}$ were recently determined by the group of Sanvito.[47,48] We have shown in one of our recent study that the detailed mechanism of this supramolecular polymerization in chlorinated solvents is very complex,[42] but it can be summarized as follows (Figure 1): (i) oxidation upon light-activation of a catalytic quantity of triarylamines to their radical cations, with concomitant reduction of the chlorinated solvent producing chloride counterions; (ii) formation (above a critical concentration) of a nucleus in a columnar arrangement involving hydrogen bonds; (iii) stacking of neutral triarylamines onto the nucleus and subsequent growth of the primary fibril; (iv) lateral secondary aggregations of fibrils by van der Waals forces to reach larger bundles of fibers. We will show hereafter that this mechanism is mainly retained even in the presence of larger substituents on the triarylamine core as it is the case for molecules **1**−**4** of this study (Figure 2).

RESULTS AND DICUSSION

Synthesis and Characterization of Triarylamine−Fullerene Conjugates. The synthetic pathway to connect the different components of conjugates **1**−**3** (Figure 2) was based on two cycloaddition reactions: a copper(I)-catalyzed Huisgen alkyne−azide 1,3-dipolar cycloaddition[49,50] between the triarylamine unit and the oligo(*p*-phenyleneethynylene) OPE linker followed by a 1,3-dipolar cycloaddition of azomethine ylide to fullerene.[51,52] Both reactions are known to be highly regioselective and to proceed with good yields. Concerning bis-fullerene **4**, only the 1,3-dipolar

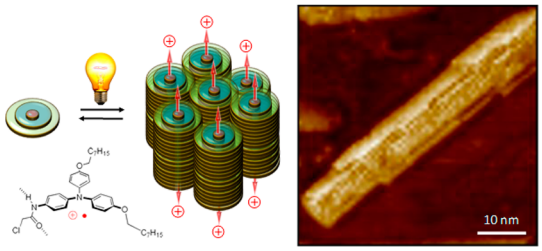

Figure 1. Schematic representation of the light-activated supramolecular polymerization of a triarylamine unit in chloroform, and its corresponding fiber structure imaged by AFM.[40]

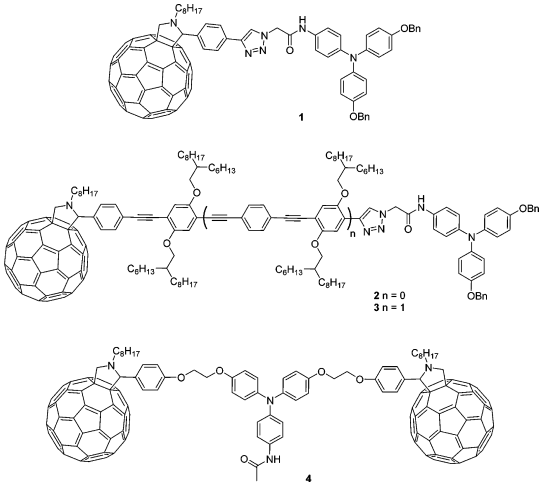

Figure 2. Chemical structures of donor−acceptor triarylamine−C_{60} conjugates 1−4.

cycloaddition of azomethine ylide was envisioned between a bis-aldehyde triarylamine derivative and C_{60} units.

Synthesis of Conjugates 1−3. The starting point for building up the three conjugates **1**−**3** was triarylamine **5** recently reported by our group (Scheme 1).[40] First, chloride derivative **5** was converted to azide **6** in the presence of sodium azide in dimethylformamide (DMF) with 91% yield after purification. Asymmetric OPE derivatives **8** and **9** were synthesized in 6 and 11 steps, respectively, from commercially available compounds and using a combination of iterative Sonogashira reactions and protecting groups manipulation.[53] Copper(I)-catalyzed Huisgen alkyne−azide 1,3-dipolar cycloaddition reactions (CuAAC) were then carried out between azide **6** and commercially available 4-ethynylbenzaldehyde or alkynes **8** or **9** to yield triazole adducts **7**, **10**, and **11**, respectively. Compounds **7** and **10** were synthesized in 91% and 64% yield, respectively, using copper iodide and triethylamine in tetrahydrofuran (THF) at room temperature. For the highly conjugated alkyne **9**, experimental conditions had to be modified to $Cu(CH_3CN)_4PF_6$ as catalyst and 2,6-lutidine as a base to yield compound **12** in good yield (65%). Prato 1,3-cycloadditions between C_{60} and

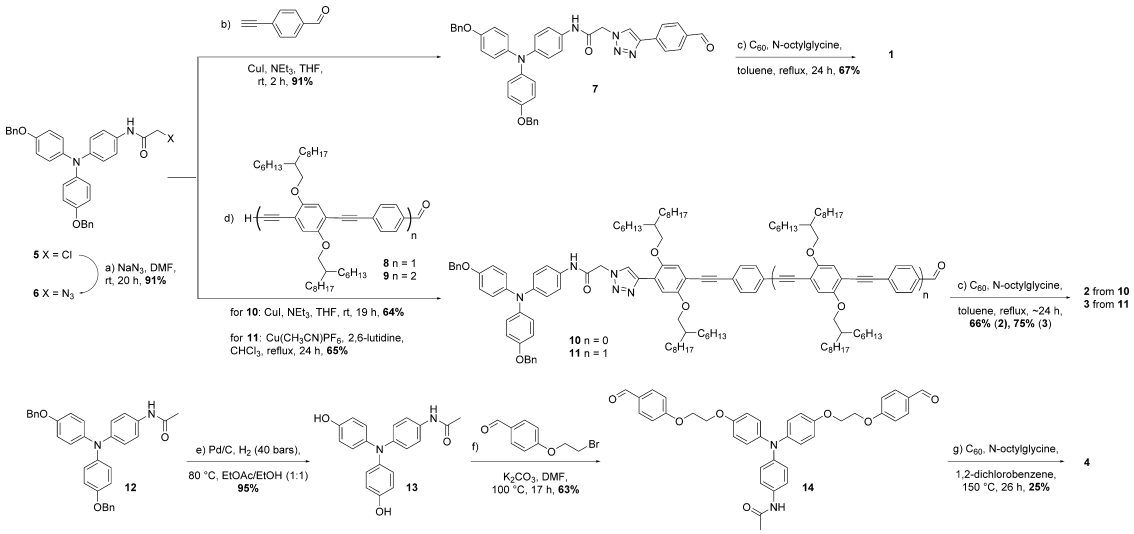

Scheme 1. Synthetic pathways for compounds 1−4.

aldehyde derivatives **7**, **10**, and **11** were finally performed under classical conditions (*N*-octylglycine, toluene, reflux) to reach fulleropyrrolidine derivatives **1** (67%), **2** (66%), and **3** (75%) in good yields.

Synthesis of Conjugate 4. First, hydrogenolysis of already synthesized compound **12**[40] was carried out with Pd/C to yield product **13** (95%). The resulting phenol moieties were then alkylated with commercially available 4-(2-bromoethoxy)benzaldehyde and K_2CO_3 in DMF at 100 °C to provide derivative **14** in 63% yield. Finally, Prato 1,3-cycloaddition between dialdehyde **14** and C_{60} in 1,2-dichlorobenzene at 150 °C for 26 h induces the formation of pyrrolidine moieties, which bear both an asymmetric center, leading to one meso isomer, and two inseparable enantiomers. However, after purification, only one of the two expected triarylamine−C_{60} conjugates was isolated in 25% yield, and the second one was inseparable from the other side-products.

Characterization of Compounds 1−4. Compounds **1**−**4** have been characterized by ^{1}H NMR, ^{13}C NMR, FTIR and ESI/MALDI-TOF mass spectra (see Materials and Methods section). Considering compound **1** as a representative example, its ^{1}H NMR spectrum in $CDCl_3$ shows all the expected resonance signals for the N−CH_2 fulleropyrrolidine group (H_K, two multiplets, 3.29−3.19 and 2.63−2.54 ppm) and the pyrrolidine hydrogens (H_I H_J, two doublets, 5.12 and 4.14 ppm, ^3J = 9.5 Hz; one singlet, 5.10 ppm), which are in good agreement with other reported *N*-alkylfulleropyrrolidine derivatives.[53−56] Furthermore, all ^{13}C spectra of derivatives **1**−**4** displayed the characteristic signals that correspond to both methyne and methylene carbon atoms of the pyrrolidine ring between δ = 83 and 67 ppm. Finally, FTIR spectra lacked the aldehyde band around 1700 cm^{-1} and mass spectra confirmed the presence of the desired final compounds.

UV−vis−NIR absorption spectra of compounds **1**−**4** (Figure 3a) and of references **6**, **S6**, **S11**, and **S14** (see Supporting Information Figure S4) were also recorded in toluene, a solvent which does not induce the formation of stable triarylammonium radical cation upon light irradiation (conversely to chloroform). We found that, below 450 nm, all reference compounds (**6**, **S6**, **S11**, and **S14**) absorb light, whereas above this wavelength, only C_{60} derivative **S14** does. Regarding the C_{60}−TAA conjugates, the electronic absorption spectra of **1** and **4** correspond well to the sum of their reference components **6** and **S14** demonstrating that no significant electronic interaction exists between the triarylamine and the fullerene moieties (Supporting Information Figure S4a,d). However, for **2** and **3**, although the shapes of both experimental and summed profiles match, differences were observed for the relative intensities of OPE $\pi-\pi^*$ bands which increase with OPE length, suggesting some degree of perturbation of the OPE transitions (Supporting Information Figure S4b,c).[57]

Similarly, fluorescence spectra of compounds **1**−**4** and their reference compounds **6**, **S6**, **S11**, and **S14** in toluene were recorded upon excitation at both 310 and 532 nm, which correspond to the maximum of absorptions of the triarylamine and C_{60} moieties, respectively (Figures 3b and S7 in Supporting Information). Upon excitation at 310 nm, a dramatic quenching of the triarylamine fluorescence contribution (λ_{em} 395 nm) was observed for compounds **1** and **4** compared to **6** under identical experimental conditions and matching optical intensity (Figure 4b). This observation might suggest an intramolecular charge-transfer from the triarylamine donor to the fullerene acceptor upon photoexcitation, a result in agreement with the literature[26,29] and in coherence with DFT calculations (*vide infra*). For compound **2**,

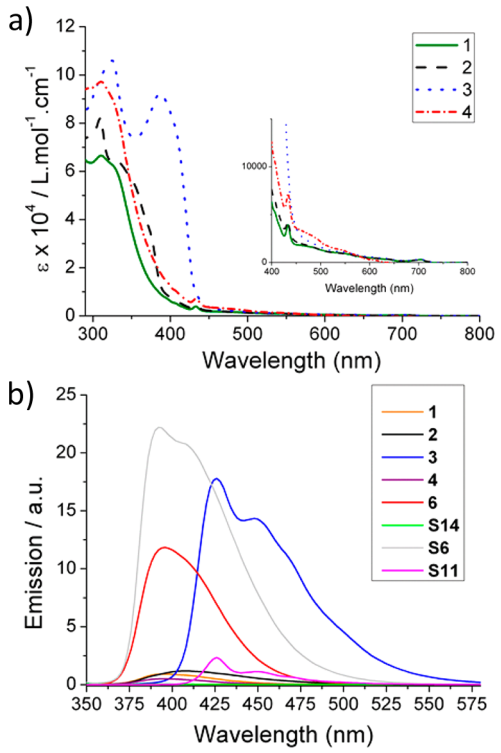

Figure 3. (a) UV−vis−NIR absorption spectra of compounds 1−4 in toluene with [1−4] = 0.01 mM. (b) Fluorescence spectra recorded upon excitation at 310 nm for compounds 1−4, 6, S6, S11 and S14.

quenching of both triarylamine and medium-length OPE fluorescence contributions was observed. However, for **3**, an enhancement of fluorescence corresponding to the long OPE linker occurrs, in addition to the quenching of the emission signal from the triarylamine moiety. When compared to **S11**, this observation suggests an energy transfer from the triarylamine to the OPE moiety. Upon excitation at 532 nm, the fluorescence of the fullerene unit was not noticeably quenched for compounds **1**−**3** compared to fulleropyrrolidine reference **S14** (Supporting Information Figure S7).

Light Irradiation Experiments in Chloroform. On the basis of our original work on light-triggered self-assembly of triarylamines in chlorinated solvents,[40−43] we then studied the possible self-assembly of our new derivatives upon light irradiation by ^{1}H NMR, optical spectroscopies, and microscopies. In particular, considering that the self-assembly process relies on the formation of a nucleus made of triarylammonium radical cations generated *in situ*,[42] we were wondering if the use of sources of light which differs by their quantity of photons would influence the structuration of our self-assemblies.

White Light Irradiation Experiments. ^{1}H NMR. Photoirradiation experiments with white light have been first followed by ^{1}H NMR, as disappearance of some NMR signals is indicative of a possible self-assembly process (Figure 4). As a representative

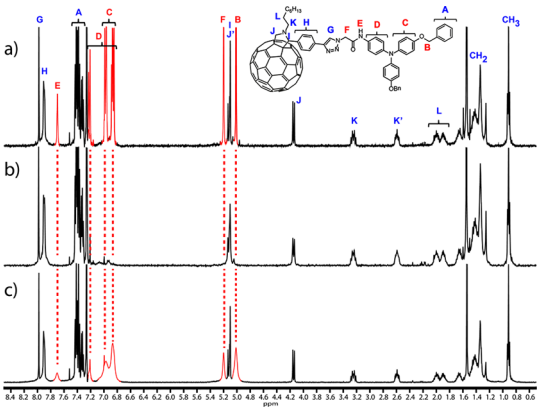

Figure 4. Typical ^{1}H NMR spectra of 1 obtained immediately after purification (a), after 4 min exposure to visible light (halogen lamp, 10 W·cm^{-2}) (b), and after subsequent heating for 22 h at 60 °C in the dark (c).

example, irradiation of a solution of **1** in $CDCl_3$ with a 20 W halogen lamp (power density of 10 W·cm^{-2}) for 4 min induces the disappearance of several resonances from the spectrum (highlighted in red in Figure 4), namely the triarylamine core protons (H_C, H_D), the benzylic CH_2 protons (H_B), the NH proton (H_E) and the acetamide protons (H_F).

Interestingly, the process was shown to be mostly reversible by simply heating the chloroform solution of **1** at 60 °C for 22 h, as illustrated by the reappearance of protons H_B-H_F (Figure 4c). This light-induced process is identical to the one observed originally for compound **5** in chlorinated solvents and is in agreement with our previous studies, revealing a strong anisotropic stacking and radical delocalization occurring through the supramolecular wires.[40−43,45] The same observations were also noticed for compounds **2**−**4** after photoirradiation and subsequent heating process (Supporting Information Figures S1−S3).

Optical Spectroscopies. To confirm the presence of the cationic radical, chloroform solutions of **1**−**4** (0.1 mM) were studied by UV−vis−NIR spectroscopy at room temperature as a function of photoirradiation (Figures 5a,b, Supporting Information S5 and S6a−c). As a representative example, white light irradiation of a solution of **1** for few minutes resulted in the appearance of an absorption band at λ_{max} = 785 nm associated with the presence of triarylammonium radical cations $\mathbf{1}^{\bullet+}$ arising from the photooxidation of the triarylamine moiety.[40−43,58,59] When plotting the absorbance intensity of the radical at 785 nm as a function of the light-irradiation time for solutions of **1**−**4**, a first increase in the absorbance followed by a slow decrease until reaching a plateau after ~40 min of irradiation is observed.

It is also evidenced that the higher the number of chromophore units per molecule (**3** > **2** > **1**), the lower the maximum of absorbance reached at 785 nm is. This observation is well correlated with the increasing

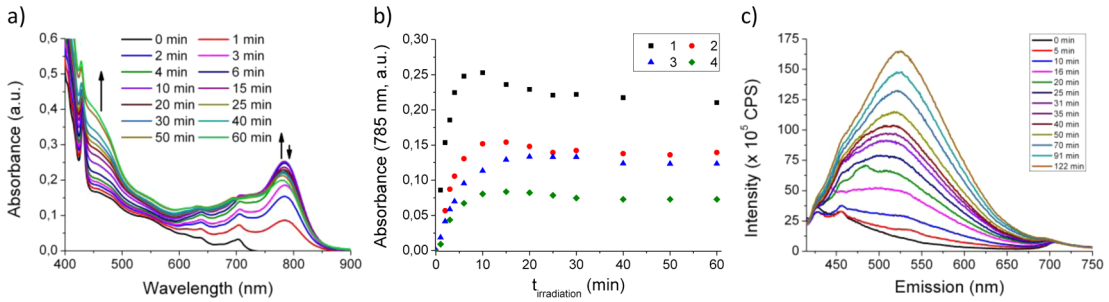

Figure 5. (a) Vis−NIR absorption spectra for compound 1 in chloroform as a function of irradiation time, [1] = 0.1 mM. (b) Irradiation kinetic experiment plotted from NIR absorption at 785 nm for 0.1 mM solutions of compounds 1−4. (c) Evolution of the fluorescence spectra of a chloroform solution of compound 1 upon excitation at 400 nm and as a function of irradiation with a halogen lamp, [1] ∼ 10^{-5} mM.

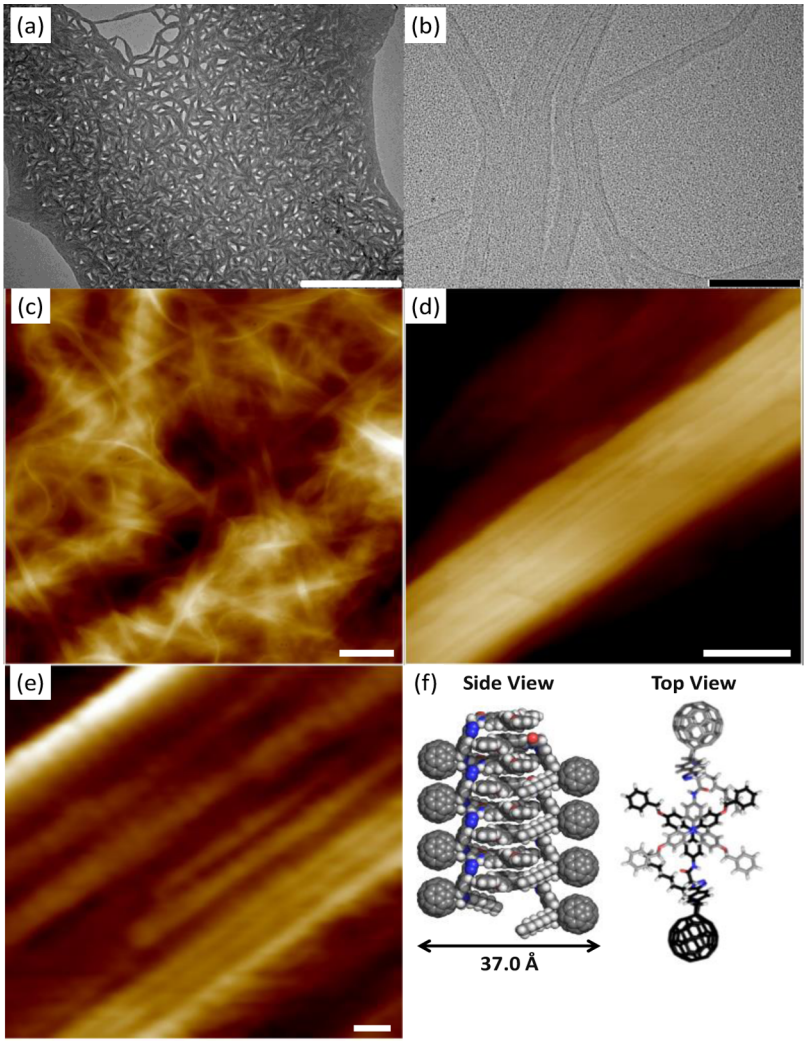

Figure 6. (a and b) TEM micrographs obtained from a chloroform solution of 1 ([1] = 0.1 mM) drop-casted onto a carbon-coated copper grid after different irradiation time with white light (scale bars: (a) 1 μm, (b) 200 nm). (c and d) AFM images of the self-assembled structures obtained from a solution of 1 irradiated with white-light for 15 min and further spin coated onto a mica surface (scale bars: (c) 2 μm, (d) 150 nm). (e) AFM imaging of an individual ribbon comprising parallel individual fibers (scale bar: 20 nm). (f) Molecular modeling of the triarylamine stacks made of 1; the calculated distance between extremities of the fullerene units was determined as ∼4 nm.

energy transfer toward the OPE linker (*vide supra*), which thus reduces the number of triarylamine moieties in the excited state available for photooxidation with chloroform.[59] For compound **1** in particular, other absorption bands centered on ∼400 and ∼460 nm and which continuously increase during light-irradiation experiments are in agreement with the formation of stacks of triarylamines, as already reported by our

group.[40−43,45] Additional fluorescence experiments on this particular molecule support this conclusion as a broad structure-less emission band from 400 to 700 nm increases with time of irradiation (Figure 5c).[45]

Microscopies. The effect of the photoirradiation on the self-assembly process was followed by TEM and AFM microscopies. Before any irradiation, TEM micrographs of chloroform solutions of **1**−**4** (0.1 mM) showed only large area of organic matter with no structuration. These solutions were then continuously irradiated with a halogen lamp (power density of 10 W·cm^{-2}) and, at precise time points, aliquots were drop-casted on TEM grids. After few minutes of irradiation, polydisperse objects were observed for **2**−**4** and no main evolution of the morphology was noticed with prolonged irradiation time (Supporting Information Figure S10). However, for **1**, after 15 min of irradiation, large areas of gel-like structures composed of entangled nanoribbons were discovered (Figure 6a). Increasing resolution shows that these ribbons are themselves composed of internally packed longitudinal fibers (Figures 6b and S9 in Supporting Information). AFM imaging of a 0.1 mM solution of **1** irradiated with white light for 15 min and then drop-casted on a mica surface confirmed the presence of these bundles of packed fibers (Figure 6c−e). By scanning the inside of the fibers using high resolution AFM, and by taking into consideration the convolution by the AFM tip, one can measure the diameter of a single fiber with a dimension of 4.9 ± 0.6 nm, which is in agreement with a monodimensional stack of triarylamines as determined by molecular modeling and showing a stable supramolecular heterojunction configuration (Figure 6e,f). Wide-angle X-ray scattering experiment confirmed this one-dimensional ordering of the molecules with large peaks at 1.38 and 2.01 Å^{-1}, which correspond to distances between nitrogen centers of adjacent triarylamines of 4.54 Å and aryl $\pi-\pi$ stacking distances of 3.13 Å, respectively, as already observed for similar triarylamine derivatives (Supporting Information Figure S12).[42,45]

UV Light Irradiation Experiments. In the course of our study, we noticed that chloroform solutions of **1** became turbid when irradiated with sunlight instead of a halogen lamp. Considering the self-assembly mechanism of triarylamine derivatives,[42] we postulated that this effect would come from the presence of a higher quantity of UV photons in sunlight and we subsequently probed this assumption.

UV−Vis−NIR Spectroscopy. To study the effect of UV light on the system, vis−NIR kinetic experiments were performed on a 0.1 mM chloroform solution of compound **1** irradiated with a 6 W 365 nm−light lamp (power density of 1 mW·cm^{-2}) (Supporting Information Figure S6d). Interestingly, an irradiation during less than 2 min resulted in the appearance of the absorption band at 785 nm but with five times more radicals

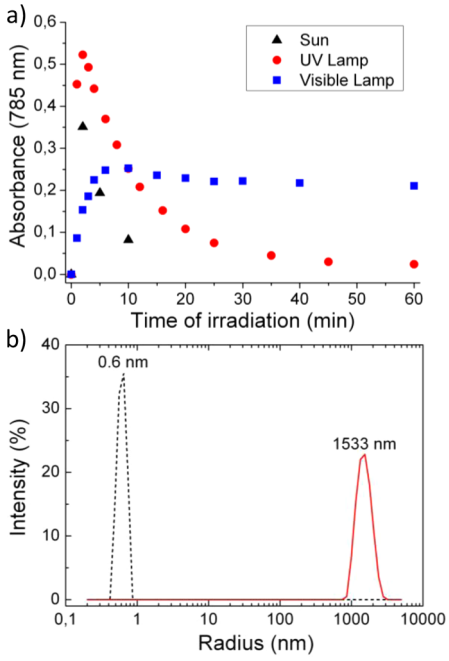

Figure 7. (a) Comparison of the evolution of the absorbance at 785 nm, as a function of time of irradiation with a halogen 20 W power lamp (■), sun (▲), and a 6 W UV lamp (●) for an initial 0.1 mM solution of 1 in chloroform. (b) Hydrodynamic radii distributions observed for compound 1 ([1] = 0.1 mM in $CHCl_3$ at T = 25 °C and θ = 173°) before irradiation (black dashed line) and after 15 min sunlight irradiation (red line).

than with the visible light irradiation on the same time scale (Figure 7a). Further irradiation induced a strong decrease of this band until reaching a plateau at a lower absorption value compared to visible light. This experiment suggests that UV light irradiation generates a higher number of radicals and therefore of nuclei necessary to prime the self-assembly process compared to white light.[42] Indeed, as radical cations can only be reduced in stacks at their extremities,[42] the strong decrease of the absorbance band at 785 nm indicates that more extremities are accessible compared to white light and therefore that a higher number of nuclei is produced. A similar observation was made when using sunlight instead of a UV lamp (Figure 7a). This is in full agreement with our theoretical model of the triarylamine self-assembly involving nucleation−growth phenomena and in which the size of the stacked objects is related to the initial intensity of the light.[42]

Light Scattering. To determine the size of the objects formed in solution with either sunlight or 365 nm UV light, dynamic light scattering measurements were carried out on a chloroform solution of compound **1** at the same concentration than used for optical spectroscopy experiments (Figures 7b and S11d in Supporting Information). A reproducible monodiperse distribution with a mean radius of 1.5 μm was measured after sunlight/UV irradiation, whereas no aggregates were detected before. Chloroform solutions of **2** and **3** also

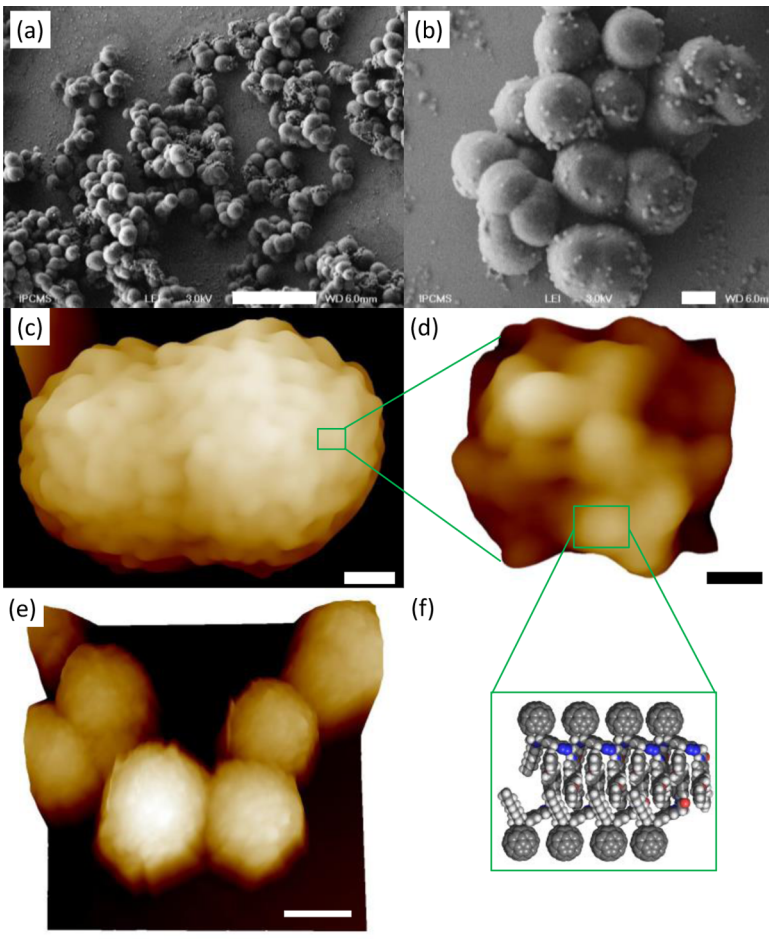

Figure 8. (a and b) SEM images obtained from a chloroform solution of 1 ([1] = 0.1 mM) irradiated time for 1 h with sunlight and drop-casted onto a silicon wafer (scale bars: (a) 10 μm, (b) 1 μm). (c−e) AFM images of the self-assembled structures obtained from a UV-light irradiated solution of 1 and spin coated onto a mica surface (scale bars: (c) 1 μm, (d) 10 nm, (e) 2 μm). (f) Molecular modeling of the triarylamine stacks made of 1; the calculated distance between extremities of the fullerene units was determined as ~4 nm.

showed the formation of aggregates with respective mean radius of 570 and 457 nm upon UV irradiation (Supporting Information Figures S11a,b). Surprisingly, whereas compound **4** did not lead to well-defined objects using white light irradiation, DLS experiment revealed the formation of polydisperse aggregates with sizes ranging from 1 to 100 μm in diameter after UV light irradiation (Supporting Information Figure S11c).

Microscopies and X-ray Scattering. A sunlight irradiated solution of **1** was drop-casted on silicon wafers and first analyzed by SEM microscopy (Figure 8a,b). A well-defined population of micrometric spheres was clearly observed, correlating the previous DLS experiments. AFM microscopy of these micrometric spheres showed a bumpy surface consisting of smaller objects in the 50−70 nm range, themselves containing a third level of organization in the 10 nm range (Figure 8c−e). One may suggest that the whole micrometric spheres are constituted of these small objects which can be considered as small monodimensional stacks of 10−20 triarylamine−fullerene conjugates and further aggregated by fullerene−fullerene interactions.[60] Indeed, wide-angle X-ray scattering (WAXS) experiment confirmed this one-dimensional ordering of the molecules with large peaks at 1.40 and 2.03 Å^{-1}, which correspond to distances between nitrogen centers of adjacent triarylamines of 4.49 Å and aryl $\pi-\pi$ stacking distances of 3.10 Å, respectively (Figures 8f and S12 in Supporting Information).[42,45] Noteworthily, attempts for visualizing objects made of **2** or **3** on surface (SEM) failed, possibly due to the disruption of the self-assemblies when interacting with the surface. Finally, SEM imaging of an irradiated solution of **4** revealed the formation of aggregates of spheres with a diameter of 1−3 μm (Supporting Information Figure S8). Although a very similar morphology was observed by SEM for self-assemblies made of **1** and **4**, DLS experiments clearly showed that in solution, spheres from **1** do not aggregate whereas spheres from **4** do. Additional WAXS experiment on **4** demonstrates the one-dimensional arrangement of the triarylamines with characteristic distances of 4.53 and 3.1 Å, similar to the ones observed previously for compound **1** (Supporting Information Figure S12). All these results

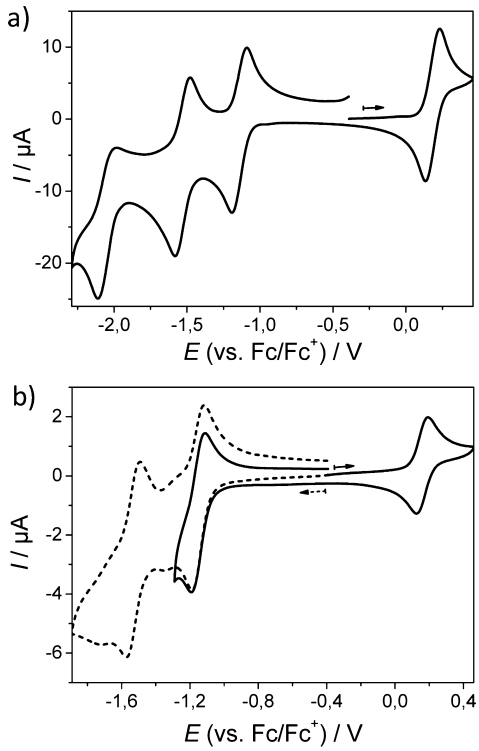

Figure 9. Cyclic voltammograms of compounds 1 (a) and 4 (b) in 0.1 M NBu_4PF_6/CH_2Cl_2 at a gold disk electrode (planar diffusion conditions). (a) 1 (c = 0.8 mM); (b) 4 ($c \approx$ 0.5 mM); solid line, cyclic voltammogram recorded in a potential window of −1.29 to 0.46 V showing the oxidation and first reduction of the TAA and C_{60} unit, respectively; dashed line, cyclic voltammogram recorded in a potential window of −0.39 to −1.79 V showing the reversible reduction of the C_{60} core to the dianion. All voltammograms were recorded with a scan rate of 100 mV·s^{-1} and were not background corrected; arrows indicate initial scan direction.

represent the first example of organic molecules in which the source of light (white light or UV) used to prime a self-assembly process can strongly influence the morphologies of the resulting supramolecular objects.

Cyclic Voltammetry. We finally investigated the electrochemical behavior of compounds **1**-**4** including the determination of reduction and oxidation potentials to define their energy levels and electronic properties. Cyclic voltammetry (CV) was recorded in solution at a gold disk electrode under planar diffusion conditions (Figures 9 and S13 in Supporting Information). Cyclic voltammograms for compounds **1**−**4** all show one chemically reversible oxidation wave corresponding to the generation of the radical cation species of the triarylamine (as confirmed by the absorption around 750 nm using *in situ* spectroelectrochemistry, Supporting Information Figures S14b, S15b, S16b, and S17b). The oxidation potential ($E_{1/2,a}$, Table 1) for compounds **1**−**3** is almost not affected by the length of the spacer, suggesting that the triarylamine core can be regarded as an isolated redox site in the TAA−C_{60} systems. For compound **4**, the anodic half-wave potential is slightly lowered compared to **1**−**3**, which can

TABLE 1. Half Wave Potentials of the Oxidation ($E_{1/2,a}$) and Reduction Processes ($E_{1/2,c}$), Energy Levels (E_{HOMO} and E_{LUMO}) and HOMO−LUMO Gap (E_{gap}) Values for Compounds 1−4[a]

	$E_{1/2,a}$ (V)	$E_{1/2,c}$ (V)[b]	E_{HOMO} (eV)[c]	E_{LUMO} (eV)[c]	E_{gap} (eV)[d]
1	+0.18	−1.14	−5.28	−3.96	1.32
		(−1.53)			
		(−2.06)			
2	+0.19	−1.15	−5.29	−3.95	1.34
		(−1.54)			
		(−2.05)			
3	+0.19	−1.15	−5.29	−3.95	1.34
		(−1.53)			
		(−2.05)			
4	+0.16	−1.15	−5.26	−3.95	1.31
		(−1.53)			
		(−2.06)			

[a] All potentials are given *vs* Fc/Fc^+; CVs were recorded at a gold electrode for concentrations between 0.5 and 0.8 mM in dichloromethane with 0.1 M $TBAPF_6$. [b] Values in parentheses correspond to the half wave potentials of the second and third reduction. [c] E_{HOMO} (= $-(E_{1/2,a} + 5.1)$ [eV]) and E_{LUMO} (= $-(E_{1/2,c} + 5.1)$ [eV]) values were calculated from the half wave potentials; for the calculation of the LUMO value, $E_{1/2,c}$ of the first redox couple was used; the error in potential values is estimated to be $\leq \pm 0.01$ V. [d] E_{gap} calculated from the HOMO and LUMO levels.

be attributed to the weak electron donor effect of the amide group.

In addition, all compounds showed three chemically reversible redox couples (Figures 9 and S12 in Supporting Information) corresponding to the generation of the radical anion, the dianionic and tricationic species of the fullerene moiety (as confirmed by the absorption between 700 and 1000 nm using *in situ* spectroelectrochemistry, Supporting Information Figures S14d, S15d, and S16d). As no significant differences in the half wave potentials of the reduction processes ($E_{1/2,c}$) are observed for compounds **1**−**4** (Table 1), the C_{60} units can be regarded as isolated redox sites that are independent of the length of the spacer.

For compound **4**, electronic communication between the two covalently linked C_{60} moieties seems to be negligible since only a single peak is observed in the corresponding voltammograms for each reduction step.[61] Finally, whereas the ratio of the peak currents for the oxidation and the first reduction of compounds **1**−**3** are unity, it corresponds to ≈2:1 (reduction: oxidation) for compound **4**, a behavior which is consistent with the molecular structure of these compounds.

Using a ferrocene−ferrocenium redox couple as external standard, very similar lowest unoccupied molecular orbitals (LUMO) levels of ∼ −3.95 eV were determined for compounds **1**−**4**. This result suggests that the incorporation of an OPE bridge between the donor and the acceptor moieties does not influence the LUMO level of the molecules. The electrochemical bandgaps (E_{gap}) were then calculated from the

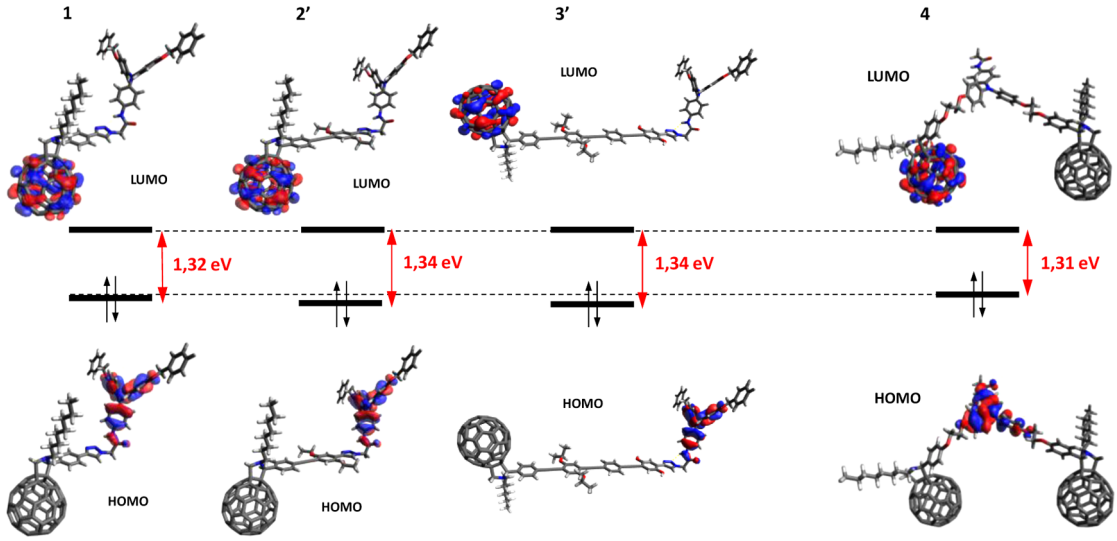

Figure 10. DFT determination of HOMO and LUMO orbitals for 1, 2′, 3′, and 4 together with bandgaps derived from cyclic voltammetric experiments (not scaled) for 1−4.

difference between the LUMO and HOMO energy levels, showing very low values comprised between 1.31 and 1.34 eV.

Molecular Modeling. We then took advantage of theoretical calculations to optimize the geometry of compounds **1**−**4** and to calculate their HOMO and LUMO surface plots (Figure 10). Their geometries were optimized by density functional theory (DFT) calculations at the B3LYP/6-31G* level of theory owing to the large dimension of the molecules.

To keep the computation feasible, the 2-hexyldecyl side chains on the OPE unit was replaced by ethyl groups for compound **2** (the resulting model being named **2**′). For compound **3**, two side chains were removed and two others were changed to isopropyl groups (the resulting model being named **3**′). The optimum geometries and the HOMO and LUMO surface plots of compounds **1**, **4** and model compounds **2**′, **3**′ are reported in Figure 10. The HOMO/LUMO orbital schemes of **1**−**3** demonstrate a strong donor−acceptor character with the HOMO consisting of a π-orbital fully delocalized over the triarylamine part, whereas the LUMO is fully centered on the fullerene moiety. Interestingly, for compound **3**, the buckyball was obtained to face the triarylamine core, *i.e.*, pointing in the opposite direction compared to compound **1** or **2**. The fact that both molecular orbitals are well separated suggests that stable charge-separated states such as $TAA^{\bullet+}$-(OPE)-$C_{60}^{\bullet-}$ could be obtained for all molecules, therefore favoring charge transfer between the donor and the acceptor units.[26,29,62] For compound **4**, both LUMO and LUMO + 1 (Supporting Information Figure S18) were found to be entirely located on the C_{60} moieties with the HOMO fully centered on the triarylamine core. This result also suggests that stable charge-separated states such as C_{60}-$TAA^{\bullet+}$-$C_{60}^{\bullet-}$ could be obtained for this compound. Moreover, we have calculated the ionization potential (Ip) and electron affinity (EA) of compound **1** resulting in values of 5.60 and 2.03 eV, respectively. Compared to a triarylamine reference (compound **S15**) whose Ip value is 5.59 eV and to a C_{60} reference (compound **S14**) whose EA value is 2.01 eV, compound **1** displays the electronic characteristics of both electroactive entities.[63] This result is in agreement with CV experiments that suggest that both TAA core and C60 unit act as isolated redox sites. Overall, both electrochemical and modeling data show that all compounds have very low and narrow HOMO−LUMO gaps (<1.40 eV), which promote them as promising molecules for efficient ambipolar charge transport.[16]

CONCLUSION

We have reported that appropriately substituted triarylamine derivatives can be associated with fullerene units in donor−acceptor conjugates while keeping their propensity to polymerize under light activation, and thus producing coaxial channels of n-type (fullerene) and p-type (triarylamine) materials. Interestingly, we show that the nanostructuration of the self-assembly can be modulated by simply changing the nature (or the intensity) of the light used to trigger supramolecular polymerization. We believe that the work described in the present article can be considered as the first example of a purely organic system in which the variation of light source/intensity can give rise to different superstructures, as it was already demonstrated and well-implemented in the nucleation growth process of inorganic nanoparticles. In that sense, it can be considered as entirely new compared to previously described example of light-sensitive self-assemblies based on cis−trans photoisomerizable units. In addition, the stimulation by light of our system leads to a highly attractive supramolecular function

where coaxial hole and electron channels are spontaneously organized up to the microscale. Finally, preliminary investigations of their structural, optical, and electrochemical properties demonstrate their potential for ambipolar charge transport and for the design of advanced and tunable supramolecular heterojunctions with potential applications in organic electronics.

MATERIALS AND METHODS

Synthesis and Characterization. All reactions were performed under an atmosphere of argon unless otherwise indicated. All reagents and solvents were purchased at the highest commercial quality and used without further purification unless otherwise noted. Dry solvents were obtained using a double column SolvTech purification system. Yields refer to purified spectroscopically (^{1}H NMR) homogeneous materials. Thin layer chromatographies were performed with TLC silica on aluminum foils (Silica Gel/UV254, Aldrich). In most cases, irradiation using a Bioblock VL-4C UV-Lamp (6 W, 254 nm and/or 365 nm) as well as Ce-molybdate stainings were used for visualization. Ultra performance liquid chromatographies coupled to mass spectroscopy (UPLC−MS) were carried out on a Waters Acquity UPLC-SQD apparatus equipped with a PDA detector (190−500 nm, 80 Hz), using a reverse phase column (Waters, BEH C18 1.7 μm, 2.1 mm × 50 mm), and the MassLynx 4.1 − XP software. MALDI mass spectra were recorded on a Bruker Daltonics Autoflex II TOF spectrometer. Elemental analyses were performed by the Service de Microanalyse, Institut Charles Sadron, CNRS. ^{1}H NMR spectra were recorded on a Bruker Avance 400 spectrometer at 400 MHz and ^{13}C spectra at 100 MHz in $CDCl_3$, acetone-d^6 or MeOD at 25 °C. The spectra were internally referenced to the residual proton solvent signal ($CDCl_3$, 7.26 ppm; acetone-d^6, 2.05 ppm; MeOD, 2.08 pm for ^{1}H spectrum; and $CDCl_3$, 77.16 ppm; acetone-d^6, 118.26 ppm; MeOD, 20.43 ppm for ^{13}C spectrum). For ^{1}H NMR assignments, the chemical shifts are given in parts per million (ppm). Coupling constants J are listed in hertz (Hz). The following notation is used for the ^{1}H NMR spectral splitting patterns: singlet (s), doublet (d), triplet (t), multiplet (m), large (l). For all experiments in chloroform (regular and deuterated), the solvent was freshly filtered on basic alumina prior to use.

Compound 1. In a 100 mL flask, C_{60} (95 mg, 132 μmol) and *N*-octylglycine[64] (49 mg, 264 μmol) were dissolved in dry toluene (25 mL) and the mixture was sonicated for 1 h. A solution of aldehyde **7** (30 mg, 44.0 μmol) was then added and the dark violet solution was heated at reflux for 24 h under argon. After removal of the solvents, the crude was purified by column chromatography (SiO_2, toluene → EtOAc/toluene: 10/90). The solid was then triturated with acetone, filtered and washed with MeOH and pentane to yield compound **1** (42 mg, 67%) as a bright black solid. R_f = 0.46 (15/85 EtOAc/toluene); ^{1}H NMR (400 MHz, $CDCl_3$, 298 K): δ = 7.98 (s, 1H), 7.95−7.83 (m, 4H), 7.70 (s, 1H), 7.44−7.29 (m, 10H), 7.22 (d, ^3J = 8.7 Hz, 2H), 6.97 (d, ^3J = 8.9 Hz, 4H), 6.89−6.84 (m, 6H), 5.20 (s, 2H), 5.12 (d, ^2J = 9.5 Hz, 1H), 5.10 (s, 1H), 5.01 (s, 4H), 4.14 (d, ^2J = 9.5 Hz, 1H), 3.29−3.19 (m, 1H), 2.63−2.54 (m, 1H), 2.05−1.94 (m, 1H), 1.94−1.83 (m, 1H), 1.71−1.26 (m, 10H), 0.91 ppm (t, ^3J = 6.8 Hz, 3H). ^{13}C NMR (100 MHz, $CDCl_3$, 298 K): δ = 162.87, 156.64, 155.08, 154.34, 153.53, 153.46, 148.39, 147.42, 146.84, 146.60, 146.41, 146.36, 146.33, 146.25, 146.04, 145.87, 145.65, 145.44, 145.37, 145.26, 144.84, 144.71, 144.53, 143.27, 143.12, 142.80, 142.68, 142.64, 142.47, 142.40, 142.21, 142.14, 142.09, 142.03, 141.92, 141.79, 141.64, 141.19, 140.31, 140.02, 139.59, 138.16, 137.16, 137.05, 136.65, 136.02, 135.83, 130.02, 129.64, 128.71, 128.11, 127.66, 126.23, 121.73, 121.66, 115.77, 82.40 (pyrrolidine CH), 70.45, 69.09, 67.02 (pyrrolidine CH_2), 53.95, 53.38 (NCH_2), 32.09, 31.09, 29.82, 29.50, 28.51, 27.76, 22.88, 14.36. FT-IR (ATR): υ = 2923, 2853, 1669, 1605, 1499, 1453, 1217, 1108, 1020, 824, 731, 694 cm^{-1}. MS (MALDI-TOF) *m/z* (%): 1532 $[M]^+$ (20), 811 $[M - C_{60}]^+$ (100), 736 $[M - C_{60} - C_5H_{11}]^+$ (38), 720 $[C_{60}]^+$ (19).

Compound 2. In a 100 mL flask, C_{60} (119 mg, 165 μmol) and *N*-octylglycine[64] (58 mg, 310 μmol) were dissolved in dry toluene (25 mL) and the mixture was sonicated for 1 h. A solution of aldehyde **10** (66 mg, 52.0 μmol) in dry toluene (6 mL) was then added and the dark violet solution was heated at reflux for 24 h under argon. The reaction mixture was then directly purified by column chromatography (SiO_2, toluene → EtOAc/toluene: 5/95). The solid was then triturated with pentane, filtered and washed with pentane and MeOH to yield compound **2** (72 mg, 66%) as a bright black solid. R_f = 0.54 (25/75 EtOAc/cyclohexane); ^{1}H NMR (400 MHz, $CDCl_3$, 298 K): δ = 8.24 (s, 1H), 7.91 (s, 1H), 7.07 (s, 1H), 7.87−7.76 (br s, 2H), 7.75−7.73 (br s, 1H), 7.59 (d, ^3J = 8.1 Hz, 2H), 7.44−7.30 (m, 10H), 7.25−7.21 (m, 2H), 7.01- 6.95 (m, 4H), 6.91−6.83 (m, 6H), 5.20 (s, 2H), 5.12 (d, ^2J = 9.4 Hz, 1H), 5.08 (s, 1H), 5.02 (s, 4H), 4.14 (d, ^2J = 9.4 Hz, 1H), 4.01 (d, ^3J = 5.5 Hz, 2H), 3.94 (d, ^3J = 5.5 Hz, 2H), 3.29−3.14 (m, 1H), 2.63−2.54 (m, 1H), 2.05−1.81 (m, 4H), 1.49−1.14 (m, 48H), 0.93 (t, ^3J = 6.9 Hz, 3H), 0.89−0.77 (m, 12H). ^{13}C NMR (100 MHz, toluene-d_8, 298 K): δ = 162.28, 156.67, 155.47, 155.38, 154.37, 153.62, 149.60, 147.53, 146.99, 146.69, 146.49, 146.14, 145.87, 145.74, 145.61, 145.46, 144.92, 144.66, 143.96, 143.39, 142.96, 142.81, 142.65, 142.54, 142.34, 142.21, 141.79, 140.46, 140.26, 139.97, 138.01, 137.73, 137.43, 137.14, 136.89, 136.24, 136.01, 132.17, 129.06, 128.82, 128.59, 128.15, 127.91, 127.67, 127.52, 126.30, 125.32, 125.08, 124.84, 122.19, 121.21, 116.69, 116.03, 113.35, 111.67, 94.41, 88.39, 82.71, 77.04, 71.95, 70.23, 69.25, 67.10, 53.49, 38.80, 32.48, 32.44, 32.39, 32.36, 32.33, 32.10, 30.69, 30.60, 30.35, 30.26, 30.22, 30.16, 29.97, 29.89, 28.88, 28.03, 27.44, 23.24, 23.21, 23.16, 20.95, 20.76, 20.57, 20.38, 20.19, 20.00, 19.81, 14.48, 14.41, 14.38. FT-IR (ATR): υ = 2921, 2851, 1666, 1605, 1539, 1498, 1452, 1423, 1376, 1216, 1106, 1019, 823, 766, 730, 693 cm^{-1}. MS (MALDI-TOF) *m/z* (%): 2111 $[M]^+$ (13), 1391 $[M - C_{60}]^+$ (100).

Compound 3. In a 100 mL flask, C_{60} (98 mg, 136 μmol) and *N*-octylglycine[64] (57 mg, 304 μmol) were dissolved in dry toluene (35 mL) and the mixture was sonicated for 1 h. A solution of aldehyde **11** (85 mg, 44.0 μmol) in dry toluene (10 mL) was then added and the dark violet solution was heated at reflux for 23 h under argon. The reaction mixture was then directly purified by column chromatography (SiO_2, toluene → EtOAc/toluene: 4/96). The solid was then triturated with acetone, filtered and washed with pentane and MeOH to yield compound **3** (92 mg, 75%) as a bright black solid. R_f = 0.69 (10/90 EtOAc/toluene); ^{1}H NMR (400 MHz, $CDCl_3$, 298 K): δ = 8.26 (s, 1H), 7.93 (s, 1H), 7.09 (s, 1H), 7.87−7.76 (br s, 2H), 7.75 (s, 2H), 7.58 (d, ^3J = 8.2 Hz, 2H), 7.51−7.47 (br s, 4H), 7.45−7.28 (m, 10H), 7.25−7.18 (m, 2H), 7.01−6.95 (m, 6H), 6.91−6.84 (m, 6H), 5.21 (s, 2H), 5.12 (d, ^2J = 9.3 Hz, 1H), 5.07 (s, 1H), 5.02 (s, 4H), 4.14 (d, ^2J = 9.3 Hz, 1H), 4.03 (d, ^3J = 5.6 Hz, 2H), 3.96 (d, ^3J = 5.6 Hz, 2H), 3.93−3.84 (m, 4H), 3.28−3.18 (m, 1H), 2.61−2.54 (m, 1H), 2.04−1.78 (m, 6H), 1.59−1.13 (m, 106H), 0.95−0.79 (m, 27H). ^{13}C NMR (100 MHz, toluene-d_8, 298 K): δ = 162.31, 156.71, 155.55, 154.62, 153.62, 149.67, 147.57, 146.55, 145.93, 145.66, 145.51, 144.72, 142.41, 141.86, 140.54, 132.24, 131.96, 127.63, 127.57, 126.36, 124.55, 122.25, 121.27, 116.11, 114.72, 113.38, 95.34, 94.49, 82.77, 77.08, 72.24, 72.06, 70.31, 69.32, 67.16, 53.54, 38.81, 32.41, 32.16, 32.09, 30.71, 30.36, 30.20, 29.97, 28.92, 28.08, 27.50, 23.23, 14.43. FT-IR (ATR): υ = 2921, 2852, 1666, 1499, 1462, 1377, 1275, 1261, 1231, 1107, 1020, 824, 749, 695, 599, 574, 552 cm^{-1}. MS (MALDI-TOF) *m/z* (%): 2791 (11) $[M]^+$, 2071 $[M - C_{60}]^+$ (100).

Compound 4. In a 100 mL flask, C_{60} (548 mg, 760 μmol) and *N*-octylglycine[64] (285 mg, 1.52 mmol) were dissolved in dry 1,2-dichlorobenzene (125 mL) and the mixture was sonicated for 1 h. A solution of aldehyde **14** (89.7 mg, 142 μmol) in dry 1,2-dichlorobenzene (15 mL) was then added and the dark violet solution was heated at 150 °C for 26 h under argon. The solvent was then distilled under reduced pressure and the crude residue was then purified by column chromatography (SiO_2, toluene → EtOAc/toluene: 50/50). The solid was then

triturated with pentane, filtered and washed with pentane and MeOH to yield compound **4** (84 mg, 25%) as a bright black solid. Only one of the two possible compounds (meso isomer and a mixture of enantiomers) was obtained with a satisfying purity. R_f = 0.73 (30/70 EtOAc/toluene); ^{1}H NMR (400 MHz, $CDCl_3$, 298 K): δ = 7.85−7.57 (br s, 4H, H_{10}), 7.29−7.24 (m, 2H, H_3 or H_4), 6.99 (d, ^3J = 8.8 Hz, 4H, H_9), 6.95 (d, ^3J = 8.9 Hz, 4H), 6.79 (d, ^3J = 8.9 Hz, 4H), 6.88 (d, ^3J = 8.8 Hz, 2H), 5.08 (d, ^2J = 9.3 Hz, 2H), 5.01 (s, 2H), 4.36−4.20 (m, 8H), 4.11 (d, ^2J = 9.3 Hz, 2H), 3.26−3.17 (m, 2H), 2.61−2.48 (m, 2H), 2.14 (s, 3H), 2.01−1.81 (m, 4H), 1.69−1.23 (m, 20H), 0.92 (t, ^3J = 6.9 Hz, 6H). ^{13}C NMR (100 MHz, $CDCl_3$, 298 K): δ = 167.9, 153.8, 147.3, 146.1, 145.9, 145.6, 145.2, 144.4, 142.6, 142.1, 130.6, 125.8, 122.3, 121.2, 115.6, 82.1, 77.2, 68.9, 66.9, 66.5, 53.1, 31.9, 29.7, 29.3, 28.3, 27.6, 22.7, 14.2; FT-IR (ATR): υ = 2921, 2849, 2790, 1674, 1605, 1463, 1430, 1367, 1303, 1220, 1171, 1103, 1069, 1039, 928, 825, 761, 718, 698, 574, 561 cm^{-1}. ESI-MS: *m/z* calculated for $C_{176}H_{72}N_4O_5$: 1161.28 $[M + 2H]^{2+}$, found 1161.27.

Additional synthetic routes and procedures for all intermediates along with NMR and ESI-MS characterization data are provided in the Supporting Information.

Characterization of the Different Self-Assemblies. ^{1}H NMR spectra before irradiation with white light and after exposure to visible light were recorded on a Bruker Avance 400 spectrometer at 400 MHz. UV−vis−NIR spectra were recorded using a Cary 500 scan Varian spectrophotometer with quartz glass cuvettes of 1 cm optical path under ambient conditions. Fluorescence spectra were recorded using a FluoroMax-4 (Horiba Jobin-Yvon) spectrophotometer with quartz glass cuvettes of 1 cm optical path under ambient conditions. Atomic force microscopy (AFM) images were obtained by scanning the samples using a Nanoscope 8 (Bruker) operated in Peak-Force tapping mode. SEM experiments were performed using a JEOL JSM-6700F FEG with a lattice resolution of 5 nm, at an accelerating voltage of 10 kV. TEM experiments were performed using a CM12 Philips microscope equipped with a MVIII (SoftImaging System) CCD camera. Samples were analyzed in Bright Field Mode with a LaB6 cathode and 120 kV tension. DLS experiments were performed using a ZetaSizer Nano ZS (Malvern Instruments, Worcestershire, U.K.) in the available size range (0.3 nm to 10 μm), except for compound **4** which was recorded on Coulter LS-100 (Beckman Coulter, Brea, CA). All cyclic voltammograms were recorded with a three electrode setup (ALS Co., Ltd., Japan) on a PGSTAT101 potentiostat (Metrohm, Germany) under argon atmosphere at room temperature in 0.1 NBu_4PF_6/CH_2Cl_2. *In situ* spectroelectrochemical absorption measurements were performed in a three electrode quartz cell[65] under thin layer conditions in reflection mode (optical path length 20−80 μm). All *ab initio* calculations were performed at the DFT level using the B3LYP functional.

Conflict of Interest: The authors declare no competing financial interest.

Supporting Information Available: Synthetic protocols for the synthesis of compounds **1**−**4**, synthetic routes and protocols for compounds **8** and **9**, characterization of all synthesized products, ^{1}H NMR spectra of compounds **2**−**4** before and after white-light irradiation, UV−vis−NIR and fluorescence spectroscopy in toluene, vis−NIR and fluorescence kinetics measurements, supplementary AFM and TEM imaging, DLS and WAXS experiments, cyclic voltammetry in solution and DFT calculations. This material is available free of charge *via* the Internet at http://pubs.acs.org.

Acknowledgment. The research leading to these results has received funding from the European Research Council under the European Community's Seventh Framework Program (FP7/2007-2013)/ERC Starting Grant agreement no. 257099 (N.G.). We wish to thank the Centre National de la Recherche Scientifique (CNRS), the COST action (CM 1304), the international center for Frontier Research in Chemistry (icFRC, fellowship to A.W.), the Laboratory of Excellence for Complex System Chemistry (LabEx CSC), the University of Strasbourg (UdS), and the Institut Universitaire de France (IUF). This work was also supported by the Agence Nationale pour la Recherche (ANR-09-BLAN-034-02, ANR-11-EMMA-009, and ANR-11-BS08-06) for postdoctoral fellowships (E.B. and J.J.C.) and by a doctoral fellowship of the Chinese Scholarship Council (G.D.). Part of this work was performed in the framework of the International Research Training Group (IRTG) "Soft Matter Science: Concepts for the Design of Functional Materials" (A.W.). We further thank the DFG for funding within the Emmy-Noether Program (S.L.). We wish to thank Guillaume Fleith (ICS) for performing WAXS experiments.

REFERENCES AND NOTES

1. Busseron, E.; Ruff, Y.; Moulin, E.; Giuseppone, N. Supramolecular Self-Assemblies as Functional Nanomaterials. *Nanoscale* **2013**, *5*, 7098–7140.
2. Bhosale, R.; Míšek, J.; Sakai, N.; Matile, S. Supramolecular n/p-Heterojunction Photosystems with Oriented Multicolored Antiparallel Redox Gradients (OMARG-SHJs). *Chem. Soc. Rev.* **2010**, *39*, 138–149.
3. Bassani, D. M.; Jonusauskaite, L.; Lavie-Cambot, A.; McClenaghan, N. D.; Pozzo, J.-L.; Ray, D.; Vives, G. Harnessing Supramolecular Interactions in Organic Solid-State Devices: Current Status and Future Potential. *Coord. Chem. Rev.* **2010**, *254*, 2429–2445.
4. Aida, T.; Meijer, E. W.; Stupp, S. I. Functional Supramolecular Polymers. *Science* **2012**, *335*, 813–817.
5. Cohen Stuart, M. A.; Huck, W. T.; Genzer, J.; Müller, M.; Ober, C.; Stamm, M.; Sukhorukov, G. B.; Szleifer, I.; Tsukruk, V. V.; Urban, M.; et al. Emerging Applications of Stimuli-Responsive Polymer Materials. *Nat. Mater.* **2010**, *9*, 101–113.
6. Russew, M.-M.; Hecht, S. Photoswitches: From Molecules to Materials. *Adv. Mater.* **2010**, *22*, 3348–3360.
7. Jochum, F. D.; Theato, P. Temperature- and Light-Responsive Smart Polymer Materials. *Chem. Soc. Rev.* **2013**, *42*, 7468–7483.
8. Yagai, S.; Karatsu, T.; Kitamura, A. Photocontrollable Self-Assembly. *Chem.—Eur. J.* **2005**, *11*, 4054–4063.
9. Yagai, S.; Yamauchi, M.; Kobayashi, A.; Karatsu, T.; Kitamura, A.; Ohba, T.; Kikkawa, Y. Control over Hierarchy Levels in the Self-Assembly of Stackable Nanotoroids. *J. Am. Chem. Soc.* **2012**, *134*, 18205–18208.
10. Hirose, T.; Helmich, F.; Meijer, E. W. Photocontrol over Cooperative Porphyrin Self-Assembly with Phenylazopyridine Ligands. *Angew. Chem., Int. Ed.* **2013**, *52*, 304–309.
11. Yagai, S.; Iwai, K.; Yamauchi, M.; Karatsu, T.; Kitamura, A.; Uemura, S.; Morimoto, M.; Wang, H.; Würthner, F. Photocontrol Over Self-Assembled Nanostructures of π-π Stacked Dyes Supported by the Parallel Conformer of Diarylethene. *Angew. Chem., Int. Ed.* **2014**, *53*, 2602–2606.
12. Jin, R.; Cao, Y. C.; Hao, E.; Métraux, G. S.; Schatz, G. C.; Mirkin, C. A. Controlling Anisotropic Nanoparticle Growth Through Plasmon Excitation. *Nature* **2003**, *425*, 487–490.
13. Klajn, R.; Bishop, K. J. M.; Grzybowski, B. A. Light-Controlled Self-Assembly of Reversible and Irreversible Nanoparticle Suprastructures. *Proc. Natl. Acad. Sci. U. S. A.* **2007**, *104*, 10305–10309.
14. Stamplecoskie, K. G.; Scaiano, J. C. Light Emitting Diode Irradiation Can Control the Morphology and Optical Properties of Silver Nanoparticles. *J. Am. Chem. Soc.* **2010**, *132*, 1825–1827.
15. Srivastava, S.; Santos, A.; Critchley, K.; Kim, K. S.; Podsiadlo, P.; Sun, K.; Lee, J.; Xu, C.; Lilly, G. D.; Glotzer, S. C.; et al. Light-Controlled Self-Assembly of Semiconductor Nanoparticles into Twisted Ribbons. *Science* **2010**, *327*, 1355–1369.
16. Samori, P.; Cacialli, F.; Anderson, H. L.; Rowan, A. E. Towards Complex Functions from Complex Materials. *Adv. Mater.* **2006**, *18*, 1235–1238.
17. Moulin, E.; Cid, J.-J.; Giuseppone, N. Advances in Supramolecular Electronics—From Randomly Self-Assembled Nanostructures to Addressable Self-Organized Interconnects. *Adv. Mater.* **2013**, *25*, 477–487.
18. Würthner, F.; Chen, Z.; Hoeben, F. J. M.; Osswald, P.; You, C.-C.; Jonkheijm, P.; Herrikhuyzen, J. v.; Schenning, A. P. H. J.; van der Schoot, P. P. A. M.; Meijer, E. W.; et al. Supramolecular

p−n-Heterojunctions by Co-Self-Organization of Oligo(p-phenylene Vinylene) and Perylene Bisimide Dyes. *J. Am. Chem. Soc.* **2004**, *126*, 10611–10618.
19. Yamamoto, Y.; Zhang, G.; Jin, W.; Fukushima, T.; Ishii, N.; Saeki, A.; Seki, S.; Tagawa, S.; Minari, T.; Tsukagoshi, K.; et al. Ambipolar-Transporting Coaxial Nanotubes with a Tailored Molecular Graphene−Fullerene Heterojunction. *Proc. Natl. Acad. Sci. U.S.A.* **2009**, *106*, 21051–21056.
20. Kira, A.; Umeyama, T.; Matano, Y.; Yoshida, K.; Isoda, S.; Park, J. K.; Kim, D.; Imahori, H. Supramolecular Donor−Acceptor Heterojunctions by Vectorial Stepwise Assembly of Porphyrins and Coordination-Bonded Fullerene Arrays for Photocurrent Generation. *J. Am. Chem. Soc.* **2009**, *131*, 3198–3200.
21. Zhang, W.; Jin, W.; Fukushima, T.; Saeki, A.; Seki, S.; Aida, T. Supramolecular Linear Heterojunction Composed of Graphite-Like Semiconducting Nanotubular Segments. *Science* **2011**, *334*, 340–343.
22. Sforazzini, G.; Orentas, E.; Bolag, A.; Sakai, N.; Matile, S. Toward Oriented Surface Architectures with Three Coaxial Charge-Transporting Pathways. *J. Am. Chem. Soc.* **2013**, *135*, 12082–12090.
23. Guldi, D. M.; Illescas, B. M.; Atienza, C. M.; Wielopolski, M.; Martin, N. Fullerene for Organic Electronics. *Chem. Soc. Rev.* **2009**, *38*, 1587–1597.
24. Urnikaite, S.; Malinauskas, T.; Gaidelis, V.; Jankauskas, V.; Getautis, V. Air-Stable, Narrow-Band-Gap Ambipolar C_{60} Fullerene−Hydrazone Hybrid Materials. *Chem.—Asian J.* **2012**, *7*, 614–620.
25. Chang, C.-L.; Liang, C.-W.; Syu, J.-J.; Wang, L.; Leung, M.-K. Triphenylamine-Substituted Methanofullerene Derivatives for Enhanced Open-Circuit Voltages and Efficiencies in Polymer Solar Cells. *Sol. Energy Mater. Sol. Cells* **2011**, *95*, 2371–2379.
26. Zalesny, R.; Loboda, O.; Iliopoulos, K.; Chatzikyriakos, G.; Couris, S.; Rotas, G.; Tagmatarchis, N.; Avramopoulos, A.; Papadopoulos, M. G. Linear and Nonlinear Optical Properties of Triphenylamine-Functionalized C60: Insights From Theory and Experiment. *Phys. Chem. Chem. Phys.* **2010**, *12*, 373–381.
27. Ouyang, X.; Zeng, H.; Ji, W. Synthesis, Strong Two-Photon Absorption, and Optical Limiting Properties of Novel C_{70}/C_{60} Derivatives Containing Various Carbazole Units. *J. Phys. Chem. B* **2009**, *113*, 14565–14573.
28. El-Khouly, M. E.; Kim, J. H.; Kwak, M.; Choi, C. S.; Ito, O.; Kay, K.-Y. Photoinduced Charge Separation of the Covalently Linked Fullerene−Triphenylamine−Fullerene Triad. Effect of Dual Fullerenes on Lifetimes of Charge-Separated States. *Bull. Chem. Soc. Jpn.* **2007**, *80*, 2465–2472.
29. El-Khouly, M. E.; Shim, S. H.; Araki, Y.; Ito, O.; Kay, K.-Y. Effect of Dual Fullerenes on Lifetimes of Charge-Separated States of Subphthalocyanine−Triphenylamine−Fullerene Molecular Systems. *J. Phys. Chem. B* **2008**, *112*, 3910–3917.
30. Sandanayaka, A. S. D.; Ikeshita, K.-I.; Rajkumar, G. A.; Furusho, Y.; Araki, Y.; Takata, T.; Ito, O. Photoinduced Intramolecular Electron-Transfer Processes in [60]Fullerene and *N,N*-Bis(biphenyl)aniline Molecular Systems in Solutions. *J. Phys. Chem. A* **2005**, *109*, 8088–8095.
31. Ramos, A. M.; Meskers, S. C. J.; van Hal, P. A.; Knol, J.; Hummelen, J. C.; Janssen, R. A. J. Photoinduced Multistep Energy and Electron Transfer in an Oligoaniline−Oligo (p-phenylene vinylene)−Fullerene Triad. *J. Phys. Chem. A* **2003**, *107*, 9269–9283.
32. Dhanabalan, A.; Knol, J.; Hummelen, J. C.; Janssen, R. A. J. Design and Synthesis of New Processible Donor-Acceptor Dyad and Triads. *Synth. Met.* **2001**, *119*, 519–522.
33. Komamine, S.; Fujitsuka, M.; Ito, O.; Moriwaki, K.; Miyata, T.; Ohno, T. Photoinduced Charge Separation and Recombination in a Novel Methanofullerene−Triarylamine Dyad Molecule. *J. Phys. Chem. A* **2000**, *104*, 11497–11504.
34. Pinzón, J. R.; Gasca, D. C.; Sankaranarayanan, S. G.; Bottari, G.; Torres, T. S.; Guldi, D. M.; Echegoyen, L. Photoinduced Charge Transfer and Electrochemical Properties of Triphenylamine I(h)-$Sc_3N@C_{80}$ Donor-Acceptor Conjugates. *J. Am. Chem. Soc.* **2009**, *131*, 7727–7734.
35. Shirota, Y. Photo- and Electroactive Amorphous Molecular Materials—Molecular Design, Syntheses, Reactions, Properties, and Applications. *J. Mater. Chem.* **2005**, *15*, 75–93.
36. Roncali, J. Molecular Bulk Heterojunctions: An Emerging Approach to Organic Solar Cells. *Acc. Chem. Res.* **2009**, *42*, 1719–1730.
37. Song, Y.; Di, C.-A.; Xu, W.; Liu, Y.; Zhang, D.; Zhu, D. New Semiconductors Based on Triphenylamine with Macrocyclic Architecture: Synthesis, Properties and Applications in OFETs. *J. Mater. Chem.* **2007**, *17*, 4483–4491.
38. Bordeau, G.; Lartia, R.; Metge, G.; Fiorini-Debuisschert, C.; Charra, F.; Teulade-Fichou, M.-P. Trinaphthylamines as Robust Organic Materials for Two-Photon-Induced Fluorescence. *J. Am. Chem. Soc.* **2008**, *130*, 16836–16837.
39. Thelakkat, M. Star-Shaped, Dendrimeric and Polymeric Triarylamines as Photoconductors and Hole Transport Materials for Electro-Optical Applications. *Macromol. Mater. Eng.* **2002**, *287*, 442–461.
40. Moulin, E.; Niess, F.; Maaloum, M.; Buhler, E.; Nyrkova, I.; Giuseppone, N. The Hierarchical Self-Assembly of Charge Nanocarriers: A Highly Cooperative Process Promoted by Visible Light. *Angew. Chem., Int. Ed.* **2010**, *49*, 6974–6978.
41. Moulin, E.; Niess, F.; Fuks, G.; Jouault, N.; Buhler, E.; Giuseppone, N. Light-Triggered Self-Assembly of Triarylamine-Based Nanospheres. *Nanoscale* **2012**, *4*, 6748–6751.
42. Nyrkova, I.; Moulin, E.; Armao, J. J.; Maaloum, M.; Heinrich, B.; Rawiso, M.; Niess, F.; Cid, J.-J.; Jouault, N.; Buhler, E.; et al. Supramolecular Self-Assembly and Radical Kinetics in Conducting Self-Replicating Nanowires. *ACS Nano* **2014**, *8*, 10111–10124.
43. Domoto, Y.; Busseron, E.; Maaloum, M.; Moulin, E.; Giuseppone, N. Control over Nanostructures and Associated Mesomorphic Properties of Doped Self-Assembled Triarylamine Liquid Crystals. *Chem.—Eur. J.* **2015**, *21*, 1938–1948.
44. Faramarzi, V.; Niess, F.; Moulin, E.; Maaloum, M.; Dayen, J.-F.; Beaufrand, J.-B.; Zanettini, S.; Doudin, B.; Giuseppone, N. Light-Triggered Self-Construction of Supramolecular Organic Nanowires as Metallic Interconnects. *Nat. Chem.* **2012**, *4*, 485–490.
45. Armao, J. J.; Maaloum, M.; Ellis, T.; Fuks, G.; Rawiso, M.; Moulin, E.; Giuseppone, N. Healable Supramolecular Polymers as Organic Metals. *J. Am. Chem. Soc.* **2014**, *136*, 11382–11388.
46. Kumar, R. H.; Churches, Q. I.; Subbiah, J.; Gupta, A.; Ali, A.; Evans, R. A.; Holmes, A. B. Enhanced Photovoltaic Efficiency *via* Light-Triggered Self-assembly. *Chem. Commun.* **2013**, *49*, 6552–6554.
47. Akande, A.; Bhattacharya, S.; Cathcart, T.; Sanvito, S. First Principles Study of the Structural, Electronic, and Transport Properties of Triarylamine-Based Nanowires. *J. Chem. Phys.* **2014**, 074301.
48. Bhattacharya, S.; Akande, A.; Sanvito, S. Spin Transport Properties of Triarylamine-Based Nanowires. *Chem. Commun.* **2014**, *50*, 6626–6629.
49. Kolb, H. C.; Finn, M. G.; Sharpless, K. B. Click Chemistry: Diverse Chemical Function from a Few Good Reactions. *Angew. Chem., Int. Ed.* **2001**, *40*, 2004–2021.
50. Meldal, M.; Tornøe, C. W. Cu-catalyzed Azide-Alkyne Cycloaddition. *Chem. Rev.* **2008**, *108*, 2952–3015.
51. Maggini, M.; Scorrano, G.; Prato, M. Addition of Azomethine Ylides to C60: Synthesis, Characterization, and Functionalization of Fullerene Pyrrolidines. *J. Am. Chem. Soc.* **1993**, *115*, 9798–9799.
52. Prato, M.; Maggini, M. Fulleropyrrolidines: A Family of Full-Fledged Fullerene Derivatives. *Acc. Chem. Res.* **1998**, *31*, 519–526.
53. Wielopolski, M.; Atienza, C.; Clark, T.; Guldi, D. M.; Martín, N. p-Phenyleneethynylene Molecular Wires: Influence of Structure on Photoinduced Electron-Transfer Properties. *Chem.—Eur. J.* **2008**, *14*, 6379–6390.
54. Yu, M.-L.; Wang, S.-M.; Feng, K.; Khoury, T.; Crossley, M. J.; Yang, F.; Zhang, J.-P.; Tung, C.-H.; Wu, L.-Z. Photoinduced Electron Transfer and Charge-Recombination in 2-Ureido-4[1*H*]-pyrimidinone Quadruple Hydrogen-Bonded

Porphyrin–Fullerene Assemblies. *J. Phys. Chem. C* **2011**, *115*, 23634–23641.
55. Segura, M.; Sánchez, L.; de Mendoza, J.; Martín, N.; Guldi, D. M. Hydrogen Bonding Interfaces in Fullerene·TTF Ensembles. *J. Am. Chem. Soc.* **2003**, *125*, 15093–15100.
56. Gu, T.; Nierengarten, J.-F. Synthesis of Fullerene–Oligophenyleneethynylene Hybrids. *Tetrahedron Lett.* **2001**, *42*, 3175–3178.
57. Clifford, J. N.; Gu, T.; Nierengarten, J.-F.; Armaroli, N. Photoinduced Energy and Electron Transfer in Fullerene-Oligophenyleneethynylene Systems: Dependence on the Substituents of the Oligomer Unit. *Photochem. Photobiol.* **2006**, *5*, 1165–1172.
58. Amthor, S.; Noller, B.; Lambert, C. UV/Vis/NIR Spectral Properties of Triarylamines and Their Corresponding Radical Cations. *Chem. Phys.* **2005**, *316*, 141–152.
59. Richtol, H. H.; Fitzgerald, E. A.; Wuelfing, P. Photochemical Oxidation of Some Substituted Aromatic Amines in Chloroform. *J. Phys. Chem.* **1971**, *75*, 2737–2741.
60. Georgakilas, V.; Pellarini, F.; Prato, M.; Guldi, D. M.; Melle-Franco, M.; Zerbetto, F. Supramolecular Self-Assembled Fullerene Nanostructures. *Proc. Natl. Acad. Sci. U.S.A.* **2002**, *99*, 5075–5080.
61. Janisch, J.; Klinkhammer, R.; Ruff, A.; Schäfer, J.; Speiser, B.; Wolff, C. Two-Electron-Transfer Redox Systems. Part 8. Proving the Electron Stoichiometry for the Electrochemical Two-Electron Oxidation of *N*,*N*′-Bis(ferrocenoyl)-1,2-diaminoethane. *Electrochim. Acta* **2013**, *110*, 608–618.
62. Chudomel, J. M.; Yang, B.; Barnes, M. D.; Achermann, M.; Mague, J. T.; Lahti, P. M. Highly Twisted Triarylamines for Photoinduced Intramolecular Charge Transfer. *J. Phys. Chem. A* **2011**, *115*, 8361–8368.
63. Newman, C. R.; Frisbie, C. D.; da Silva Filho, D. A.; Brédas, J.-L.; Ewbank, P. C.; Mann, K. R. Introduction to Organic Thin Film Transistors and Design of n-Channel Organic Semiconductors. *Chem. Mater.* **2004**, *16*, 4436–4451.
64. Li, J.; Grennberg, H. Microwave-Assisted Covalent Sidewall Functionalization of Multiwalled Carbon Nanotubes. *Chem.—Eur. J.* **2006**, *12*, 3869–3875.
65. Geskes, C.; Heinze, J. A Spectroelectrochemical Cell for Measurements in Highly Purified Solvents. *J. Electroanal. Chem.* **1996**, *418*, 167–173.